Applied Geochemistry 157 (2023) 105777

Contents lists available at ScienceDirect

Applied Geochemistry

journal homepage: www.elsevier.com/locate/apgeochem

Magnesium isotope fractionation during natural travertine deposition from Baishuitai, SW China

Jincun Liu [a], Jiubin Chen [a,*], Zhengrong Wang [b], Hongming Cai [a], Wei Yuan [a], Zhongwei Wang [c], Fang Huang [d], Congqiang Liu [a]

[a] Institute of Surface-Earth System Science, School of Earth System Science, Tianjin University, Tianjin, 300072, China
[b] Department of Earth & Atmospheric Sciences, The City College of New York, CUNY, New York, 10031, USA
[c] State Key Laboratory of Environmental Geochemistry, Institute of Geochemistry, Chinese Academy of Sciences, Guiyang, 550081, China
[d] CAS Key Laboratory of Crust-Mantle Materials and Environments, School of Earth and Space Sciences, University of Science and Technology of China, Hefei, Anhui, 230026, China

ARTICLE INFO

Editorial Handling by: Dr. Zimeng Wang

Keywords:
Travertine
Mg isotopes
Fractionation mechanisms
Temperature effect
Paleoenvironment reconstruction

ABSTRACT

Travertine samples deposited in Earth's surface environments can be used as an effective archive for paleo-climatic reconstruction. As a common element in carbonates, magnesium (Mg) and its isotopic composition in travertine could provide useful information for evaluating paleo-environment changes. In this study, we investigate the Mg isotope systematics in both endogenic travertines (mainly calcite) and spring/stream waters at Baishuitai, Yunnan, SW China. Our results show a systematic increase in δ^{26}Mg value from −1.37 to −1.26‰ for water samples downstream, but varied δ^{26}Mg values between −4.12 and −3.95‰ (average −4.02‰) for solid carbonates, thus a corresponding fractionation $\Delta^{26}Mg_{calcite\text{-}water}$ between −2.76 to −2.59‰ (mean value of −2.69‰). Therefore, the solid carbonates preferentially incorporate light Mg isotopes during travertine formation. More interestingly, the Mg distribution coefficient ($K_{Mg/Ca}$) between travertine and water exhibits two variation trends with the calcite deposition rate (R_p) along the canal, which can be explained by the change of calcite formation mechanism from direct nucleation to precipitation via amorphous calcium carbonate (ACC) intermediate. In the upper-stream, the direct nucleation of calcite results in the rapid incorporation of Mg ions into crystal lattice, while a relatively slow precipitation of calcite downstream would incorporate Mg *via* ACC formation pathway in a quasi-equilibrium pattern. This is consistent with the grain size distribution and crystal morphology observed under SEM. Our results show the important control of water Mg/Ca ratios on the calcite precipitation during travertine formation, and imply the potential and complexity of using Mg isotopes of travertine deposits to reconstruct paleo-environments.

1. Introduction

Travertine and tufa are terrestrial supergene carbonates formed in riverine, lacustrine, marshy and spring settings, and may be used as effective archives for reconstructing climatic condition changes on continents (e.g., Dong et al., 2023; Kano et al., 2019; Liu et al., 2003; Liu et al., 2006a; Liu et al., 2010; Minissale et al., 2002; Pentecost, 2005; Yan et al., 2017). The travertine deposition generally occurs due to the degassing of carbon dioxide (CO_2) from carbonate-supersaturated aqueous solutions which generally originate from intense interactions between rocks and meteoric water, surface water or ground water. The high partial pressure of CO_2 (pCO_2) in aqueous solution could be sourced from atmosphere, soil biogenesis, and decarbonation of carbonate rocks (e.g., Kano et al., 2019). Travertine normally grows rapidly (mm to cm per year), which is about two orders of magnitude faster than tufa, and therefore, has great potential for investigating the paleo-climate with much higher (even daily) resolution (e.g., Kano et al., 2019; Liu et al., 2010; Pentecost, 2005).

The paleo-climatic information can be recorded in physicochemical parameters (including the lamina thickness and texture), elemental content, and corresponding stable isotope compositions of travertine (e.g., De Boever et al., 2017; Fernandez-Martinez et al., 2017; Kano et al., 2019; Liu et al., 2010; Sun and Liu, 2010; Sun et al., 2014; Wang et al., 2014; Watkins et al., 2014; Yan et al., 2012; Yan et al., 2016). Among

* Corresponding author.
E-mail address: jbchen@tju.edu.cn (J. Chen).

https://doi.org/10.1016/j.apgeochem.2023.105777
Received 6 May 2023; Received in revised form 21 August 2023; Accepted 22 August 2023
Available online 28 August 2023

these parameters, oxygen (O) and carbon (C) isotope fractionations between travertine and coexisting water are the most intensively-studied paleo-proxies to date (e.g., Andrews, 2006; Kano et al., 2019; Mutlu et al., 2022; Sun et al., 2022; Yan et al., 2016). Recently, Yan et al. (2016) reported the significant correlation of Ca isotope compositions of calcite with those of ambient water from the Baishuitai travertine deposition system and proposed that Ca isotopes may be a useful tool for tracking past hydrodynamic variations. Since the stable isotope compositions of travertine (including C, O and Ca) are likely affected by various environmental factors and it is difficult to directly linking the measured isotopic variations in travertine with specific environmental changes, multiple proxies may be helpful to better constrain environmental factors effectively.

Mg is a relatively-abundant trace element in travertine. Its isotope composition may provide additional information on the mechanisms of travertine deposition due to its high hydration energy compared with other metal ions in aqueous environment and its retarding effect on calcite surface during crystallization (Berner, 1975). Previous studies have shown that Mg isotope fractionation during abiogenic and biogenic carbonate precipitations may be impacted by multiple factors such as the precipitation temperature (e.g., Galy et al., 2002; Li et al., 2012; Liu and Li, 2022), precipitation rate (e.g., Mavromatis et al., 2013), fractionation mechanism (e.g., Buhl et al., 2007; Mavromatis et al., 2017), potential Mg^{2+} speciation (Schott et al., 2016), mineralogy of carbonate precipitates (e.g., Geske et al., 2012; Geske et al., 2015; Immenhauser et al., 2010; Saulnier et al., 2012; Wombacher et al., 2011), organic *vs.* inorganic precipitation (e.g., Chang et al., 2004; Pogge von Strandmann, 2008; Saenger and Wang, 2014), and vital effects (e.g., Balland-Bolou-Bi et al., 2019; Black et al., 2006; Black et al., 2007; Black et al., 2008; Bolou-Bi et al., 2010; Bolou-Bi et al., 2012; Kimmig et al., 2018; Opfergelt et al., 2014; Ra and Kitagawa, 2007; Ra et al., 2010a, b; Tipper et al., 2010; Wrobel et al., 2020). A few field investigations on continental carbonate samples also reported complex Mg isotope variations (e.g., Buhl et al., 2007; Galy et al., 2002; Immenhauser et al., 2010; Pogge von Strandmann et al., 2019; Riechelmann et al., 2012). For example, Galy et al. (2002) and Buhl et al. (2007) investigated $\delta^{26}Mg$ values of calcitic speleothems in 5 caves (one in the French Alps, three in Israel, and one in NW Africa of Morocco) and found that they vary little with temperature, but more with local source signature. Similarly, Riechelmann et al. (2012) reported $\delta^{26}Mg$ time-series on speleothems collected at different climatic conditions and showed that Mg isotope systematics may be affected less by temperature change, but more by the sources of Mg. However, Immenhauser et al. (2010) measured $\delta^{26}Mg$ values of a speleothem from a monitored cave in Germany and found that the large $\delta^{26}Mg$ variation in these calcite samples mainly indicate the change of the precipitation rate, with smaller fractionation occurring during faster calcite precipitation. More recently, Pogge von Strandmann et al. (2019) reported the $\delta^{26}Mg$ values of travertines precipitated from Icelandic river (Hvanná) impacted by the Eyjafjallajökull volcano, and suggested that the variation of $\delta^{26}Mg$ together with pH and Sr/Ca ratio would be controlled also by the precipitation rate.

In this study, we investigate Mg isotope systematics in the endogenic travertine deposition system at Baishuitai, Yunnan, SW China, with samples collected along a canal, where the variations of hydrochemistry, travertine deposition rates, C and O isotope ratios have been systematically-characterized in both temporal and spatial scales (Liu et al., 2003, 2006a, 2006b, 2010; Sun et al., 2014; Sun and Liu, 2010; Yan et al., 2012). We examine the variations of $\delta^{26}Mg$ values of both stream/spring water and travertine deposits along the canal, discuss the processes and mechanisms fractionating Mg isotopes, and assess the potential of Mg isotopes for constructing the paleo-environment and paleo-climate variables.

2. Geological background

The Baishuitai travertine system (N27°35′, E100°21′) is located in the Baidi village, Shangri-La county, Yunnan province, SW China (Fig. 1), with the elevation ranging from 2380 to 3900 m above sea level (MASL). This area is characterized by a subtropical monsoon climate, which results in more than three quarters of the annual precipitation (~714 mm) occurring during the rainy season from June to October (e.g., Liu et al., 2003; Liu et al., 2006a; Liu et al., 2010; Sun et al., 2014; Sun and Liu, 2010; Wang et al., 2020; Yan et al., 2012; Yan et al., 2016; Yan et al., 2017). The climate and natural vegetation at the site vary with altitude on the mountain slope and the mean annual temperature is ~8 °C at the sampling altitude (Wang et al., 2020). Limestone, shale and sandstone of mid-Triassic Beiya Formation are the main rock types in this area and a series of crack and karst caves are well-developed due to the tectonic movement and karstification (e.g., Liu et al., 2006b; Wang et al., 2020; Yan et al., 2016). The water-limestone interactions not only produce channels for spring water, but also provide ions (for example Ca^{2+}, Mg^{2+}, and HCO_3^-) for travertine formation.

3. Sampling and analytical methods

3.1. Sampling

Samples were collected downstream along the canal over a distance of ~2600 m and descending from 2900 to 2600 MASL as shown in Fig. 1. The width of the canal spans from 30 to 70 cm and the depth ranges from 10 to 20 cm. The flow rate in the canal ranges from 50 to 70 L/s (Liu et al., 2010).

In this study, the sampling was performed in winter for following two reasons: First, the regional precipitation at Baishuitai in winter is significantly lower than in summer, and no rainfall occurred during the sampling period of this study, reducing the effect of dilution and atmospheric precipitation (Liu et al., 2006; Liu et al., 2010; Sun and Liu, 2010; Yan et al., 2016). Second, blue-green algae were frequently found in travertine samples in summer, which may impact on Mg concentration and its isotope compositions of river water and travertine given the fact that Mg is an essential element for chlorophyll in photosynthetic organisms (Black et al., 2006; Black et al., 2007; Ra et al., 2010; Young and Galy, 2004). The samples were collected between December 2nd and 30th of year 2013 when the mean monthly temperature (2–5 °C) was the lowest of the year. The color of travertine in our study is close to pure white (*vs.* dark color for those deposited in summer). During leaching, there was almost no final leaching residue, which indicates that the supply of exogenous materials was limited. No algae were observed in SEM images of travertine samples.

Spring water originates from site $S_{1\text{-}3}$ and stream waters were sampled at sites WW_1 through WW_{11} at an approximately equal interval along the canal. Water samples were filtered through ~0.45 μm Millipore express membrane filters immediately after sampling, the filtered water is then acidified to pH = 2 with double-distilled clean nitric acid and stored in precleaned polypropylene bottles (Nalgene, America) at ~4 °C.

Travertine samples were collected at site WW_1 through WW_{11} following the sampling method reported previously (e.g., Gradziński, 2010; Kano et al., 2019; Kele et al., 2015; Sun et al., 2014; Sun and Liu, 2010; Wang et al., 2014; Wang et al., 2020; Yan et al., 2012; Yan et al., 2016). A 15 × 15 cm plexiglass slide was placed in the flowing water (~8 cm depth, in the middle of the canal) to collect travertine samples along the canal over the entire sampling period (29 days) at 11 sampling sites (WW_1–WW_{11}). After collection, travertine samples were scraped off plexiglass slides with an acid-cleaned ceramic knife, and then stored in an acid-cleaned 50 ml centrifuge tube.

3.2. Measurement of hydrogeochemical parameters and travertine deposition rate

The pH and temperature of water samples were measured in the field using a hand-held multiparameter analyzer (WTW 3430, WTW,

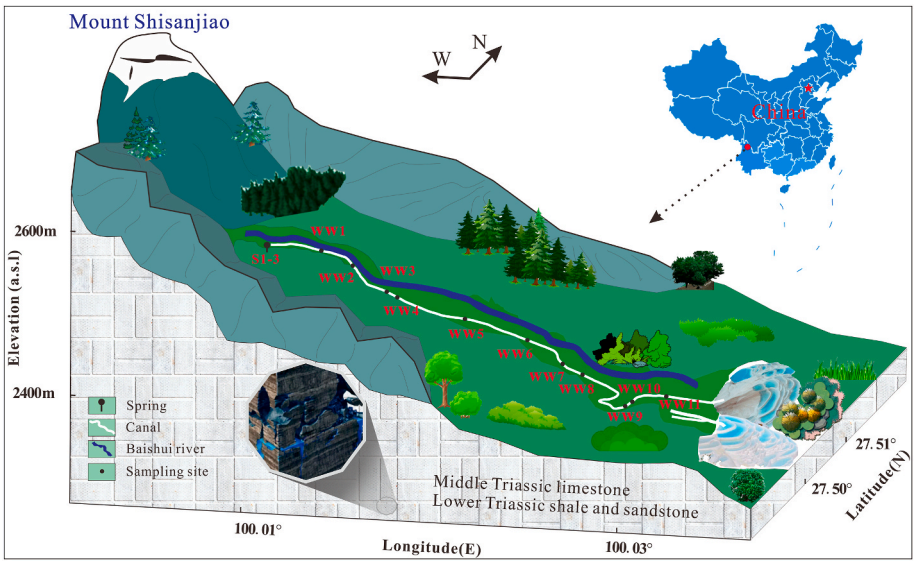

Fig. 1. Location of sampling sites along the canal of the travertine deposition system at Baishuitai, Yunnan, SW China.

Germany) with resolutions of 0.004 and 0.2 °C, respectively. The concentrations of HCO_3^- were measured by titration on site via an alkalinity test kit with an analytical resolution of approximately 6 mmol/L. The concentrations of cations (including Ca^{2+} and Mg^{2+}) in the filtered water samples were measured using the ICP-OES with a precision generally better than 10%. Before analyses, they were first dried overnight on the hot plate at ~90 °C and the residuals were re-dissolved in ~5% nitric acid in the clean lab. The PHREEQC software with the MINTEQ V4 database was used to calculate the speciation of carbon, the partial pressure of CO_2 (pCO_2), and the saturation index (SI) of calcite, based on the measured hydrochemical parameters of water samples.

The mineral composition and surface morphology of deposited travertine samples were analyzed using an X-ray diffractometer (XRD, Empyream, Malvern Panalytical, Netherlands) and scanning electron microscope (SEM, Sigma 500, Zeiss, Germany), respectively. The average travertine deposition rate (R_p) was calculated from the dry weight of solid (calcite), the upper surface area of plexiglass substrates and sampling time (e.g., Kano et al., 2019; Sun et al., 2014; Wang et al., 2020; Yan et al., 2012; Yan et al., 2016) as follows:

$$R_p = (Wt_1 - Wt_0) / (S \times t) \quad (1)$$

where Wt_1 and Wt_0 are weights of plexiglass substrates after and before each collection, respectively, S is the surface area of the substrate (~225 cm^2) and t is travertine collection duration.

3.3. Step-leaching of travertine sample

As surface absorption and the possible presence of clay and evaporite minerals may affect the result of Mg isotope compositions of carbonates in travertine samples, we conducted a step-leaching procedure on the solids to extract the elements of interest only from carbonates. The protocol was modified after Liu et al. (2013). Briefly, about 50 mg of dry travertine samples were sequentially treated using ~10% methanol (v/v) and 1 N NH_4Ac (pH = 7), respectively, to remove the potential organic matter and surface absorbed Mg^{2+}. The solid residuals after leaching were then dissolved in ~40 ml of ~0.25% HAC. The supernatants were collected for measuring elemental concentrations and Mg isotope ratios. During each leaching step, the sample was sonicated at room temperature for 10 min, followed by centrifugation at 3800 rpm for 10 min.

3.4. Purification and isotopic measurement of Mg

The purification and analytical methods for Mg isotope analyses are modified after An et al. (2014). In brief, an aliquot of supernatant after leaching (containing ~20 μg Mg) was dried first, dissolved in ~2 N HNO_3, and then passed through a cation exchange column (Biorad AG50W-X12, 200–400 mesh) twice to purify Mg in a class-1000 clean lab equipped with a class-100 laminar flow exhaust hood at Tianjin University (TJU) and University of Science and Technology of China (USTC) (Figure SI 1). In this study, ~2 N HCl was used as eluent acid to separate Mg^{2+} from Ca^{2+} with high yield (~100%) (Figure SI 2). Since calcites in travertine samples have high Ca/Mg ratios, and Ca^{2+} impurity may introduce possible interferences during Mg isotope measurement using MC-ICP-MS (i.e., Ca contamination can significantly reduce the measured $\delta^{26}Mg$ value, e.g., Galy et al., 2002), we repeated the purification procedure twice using the same columns. The total Mg blank for the purification process is generally less than 10 ng, introducing an uncertainty in the $\delta^{26}Mg$ value by less than 0.05‰.

The measurements of isotopic compositions of Mg in water and calcite were carried out at TJU and USTC using MC-ICP-MS (NEPTUNE Plus). All measurements were run at least in triplicate and the concentration of Mg is fixed to ~400 ppb to obtain ~10 V for ^{24}Mg. The standard-sample bracketing (SSB) technique was consistently applied to reduce the effect of signal drifts and correct the instrumental mass-bias, and all data are presented as $\delta^{26}Mg$ with respect to the pure magnesium metal reference material (DSM-3) provided by Dead Sea Magnesium Ltd., Israel (Galy et al., 2003):

$$\delta^{26}Mg\ (‰) = [(^{26}Mg/^{24}Mg)_{sample}/(^{26}Mg/^{24}Mg)_{DSM\text{-}3} - 1] \times 1000 \quad (2)$$

Our long-term external analytical reproducibility of $\delta^{26}Mg$ is typically better than 0.10‰ (2SD) based on repeated measurements of the standards CAM-1 (−2.62 ± 0.10‰, 2SD; N = 5) and IGG-Mg (−1.75 ± 0.04‰, 2SD; N = 3) over the course of this study, and these values are consistent with previously reported results (e.g., An et al., 2014; Mavromatis et al., 2021; Teng, 2017). The MC measurements of standards at both TJU and USTC labs gave identical values. The carbonate reference materials stalagmite (SS) and IAPSO seawater (NASS-6) were processed and measured using the identical protocols to the travertine and water samples, which gave the $\delta^{26}Mg$ values of −4.14 ± 0.04‰ (2SD, n = 6) and −0.84 ± 0.03‰ (2SD, n = 3), respectively, in agreement with literature values (An et al., 2014; Teng et al., 2015; Teng, 2017; Zhao et al., 2019).

4. Results

4.1. Variation of hydrogeochemical parameters

Table 1 and Fig. 2 present measured and calculated hydrochemical parameters along the canal. The measured mean water temperature (T) decreases from 6.2 °C to 1.5 °C downstream (Fig. 2a). The pH value is 8.0 for the water sample at WW_1, increases to 8.2 at WW_3 (~730 m away from WW_1), varies slightly between WW_3 through WW_8, and then decreases to ~8.0–8.1 at WW_9 through WW_{11} (Fig. 2a). The concentration of Ca^{2+} in the water sample decreases continuously from 5.0 mmol/L at WW_1 and WW_2 to 2.7 mmol/L at WW_6, as a result of travertine deposition (Fig. 2c). The XRD analyses showed that calcite is the main mineral phase in these travertine samples, consistent with previous studies (e.g., Liu et al., 2006a; Wang et al., 2020; Yan et al., 2016).

Calculation results show that the spring water at WW_1 is oversaturated with calcite ($SI_{WW1} = 1.1$), and the SI of spring/stream water decreases as the water flows downstream (Fig. 2b). The water spontaneously releases aqueous CO_2 to the atmosphere (CO_2 degassing) because the partial pressure of CO_2 in the epigean atmosphere (~41.5 Pa) is at least an order of magnitude lower than the pCO_2 in the water (Fig. 2b). Continuous degassing and calcite precipitation downstream reduce the partial pressure of CO_2 in the water from 349 Pa at WW_1 to 166 Pa at WW_7 (~1.8 km downstream), accompanied by the decrease of calcite saturation state (i.e., from 1.3 in WW_2 to 0.8 in WW_{11}, Fig. 2b). Moreover, the deposition rate of solid travertine (R_p) varies slightly at WW_1 through WW_5, and then decreases rapidly between WW_6 through WW_{11} (Fig. 2d). The exchange coefficient of Mg relative to Ca ($K_{Mg/Ca} = \{[Mg^{2+}]/[Ca^{2+}]\}_{calcite}/\{[Mg^{2+}]/[Ca^{2+}]\}_{water}$) between calcite and water (0.0049–0.0108) decreases first, reaches the minimum at WW_6 (0.0049), and then increases to 0.0880 along the canal (Fig. 2).

4.2. Downstream variation of Mg and its isotope composition

The Mg content of all water samples varies from 0.56 to 0.65 mmol/L, with an average value of 0.60 mmol/L (Table 1 and Fig. 2c). Unlike Ca^{2+}, Mg^{2+} concentration in the water sample has no significant decreasing trend downstream, with only small fluctuations around the average value (Fig. 2c), due probably to a very low fraction of aqueous Mg^{2+} incorporated into the solid phase (<0.19 mol%).

Mg isotope compositions of spring/stream water and calcite samples ($\delta^{26}Mg_{water}$ and $\delta^{26}Mg_{calcite}$, respectively) are shown in Table 2 and Fig. 3. Spring and stream waters exhibit a relatively small range of $\delta^{26}Mg_{water}$ values (−1.37 to −1.26‰) and show a general increase of $\delta^{26}Mg_{water}$ downstream. In contrast, $\delta^{26}Mg_{calcite}$ values of travertine samples span a limited range between −4.20‰ and −3.92‰, with an average value of −4.04‰ in the canal system. But no clear trend can be noticed.

Our data show that calcite minerals are significantly enriched in light Mg isotopes compared with coexisting spring/stream water, which is consistent with previous studies and is a typical feature of isotopic fractionation of divalent metals in carbonate minerals (including Mg, Ca, Sr, e.g., Liu et al., 2018; Tang et al., 2008a; Tang et al., 2008b; Tang et al., 2012; Yan et al., 2016). The Mg isotope fractionation factors between calcite and coexisting water ($\Delta^{26}Mg_{calcite\text{-}water}$) in our samples range from −2.76‰ to −2.59‰, with a mean value of −2.69‰, which is consistent with the Mg isotope fractionation obtained by Li et al. (2012) and Chen et al. (2020) in the lab, but different from those reported for calcites in the natural systems as reported by Immenhauser et al. (2010) and Pogge von Strandmann et al. (2019). In addition, there were no macroscopic algal mats or biofilms observed in spring/stream water and travertine during our sampling period. As such, the effect of biological activity on Mg isotope fractionation is negligible.

5. Discussion

5.1. Mg partition and calcite deposition pathway

Fig. 4 shows that the exchange coefficient $K_{Mg/Ca}$ and deposition rate R_p (both in logarithm) are roughly negatively correlated for samples collected at WW_1 through WW_6 ($R^2 = 0.34$) and at WW_6 through WW_{11} ($R^2 = 0.78$), but have significantly different slopes and R_p variation ranges. Due to the difficulty of measuring true surface area of precipitated crystals limited by our sampling method and the time-lag between the precipitation and deposition, the deposition rate (R_p) estimated is much higher and not quantitively comparable with precipitation rate (r_p) measured in previous studies (Immenhauser et al., 2010; Li et al., 2012; Mavromatis et al., 2013; Chen et al., 2020), but it is consistent with the results of Yan et al. (2017) in the same sampling system. A rough estimate of precipitation rate (r_p) based on the average crystal size and shapes measured under SEM suggest that log r_p is in the range between −7.74 and −7.66, which is similar with previous studies of calcite precipitation rate in field work and experimental simulation (Immenhauser et al., 2010; Li et al., 2012; Mavromatis et al., 2013; Chen et al., 2020).

Although the relationship between precipitation rate and deposition rate can be complex, qualitatively, they should be inversely correlated. When the crystal size is small, the precipitation rate under the same saturation state would be bigger due to larger surface, but the deposition rate would be lower for smaller crystal size under the same hydrodynamic condition. This can explain the negative correlation between log $K_{Mg/Ca}$ and log R_p (deposition rate) in this study, but a positive correlation between log $D_{Mg/Ca}$ and r_p (precipitation rate). Thus, our observation is consistent with the result of Mavromatis et al. (2013), which showed that log $K_{Mg/Ca}$ and log r_p (precipitation rate) are linearly correlated during calcite precipitation, although two trends have been

Table 1
The hydrochemical compositions for both spring/stream water and travertine samples.

Sample name	Distance (km)	Spring/stream water										Travertine		Log$K_{Mg/Ca}$ (mol/mol)
		T (°C)	pH	pCO_2 (Pa)	LogR_p (mol/s/m^2)	SI	Mg^{2+}	Ca^{2+}	HCO_3^-	CO_3^{2-}(*10^{-5})	Mg/Ca (mol/mol)	Mg^{2+}	Ca^{2+}	
							mmol/L					mmol/L		
WW_1	0.23	6.2	7.98	349	−5.14	1.10	0.61	4.76	7.50	2.74	0.13	13.48	9783	−1.97
WW_2	0.40	5.9	8.12	244	−5.12	1.26	0.59	5.26	7.38	3.71	0.11	11.13	10032	−2.01
WW_3	0.73	5.5	8.21	188	−5.10	1.23	0.59	4.20	6.94	4.11	0.14	12.80	9780	−2.03
WW_4	0.81	5.4	8.14	213	−5.20	1.21	0.56	4.87	6.73	3.46	0.12	11.99	10241	−1.99
WW_5	1.06	6.1	8.18	187	−5.09	1.17	0.63	4.02	7.37	3.57	0.16	10.64	9778	−2.16
WW_6	1.40	5.1	8.20	172	−5.24	1.01	0.65	2.75	6.06	3.41	0.24	11.45	9978	−2.31
WW_7	1.80	4.2	8.18	166	−5.38	1.01	0.60	3.16	5.67	3.02	0.19	12.30	9925	−2.19
WW_8	1.99	3.6	8.16	176	−5.46	1.00	0.60	3.26	5.78	2.89	0.18	14.55	9774	−2.09
WW_9	2.40	2.4	8.05	218	−6.00	0.83	0.60	3.11	5.55	2.05	0.19	18.79	10460	−2.03
WW_{10}	2.45	2.2	8.13	180	−5.83	0.85	0.59	2.73	5.51	2.44	0.22	19.01	9939	−2.06
WW_{11}	2.63	1.5	8.09	189	−5.67	0.80	0.62	2.82	5.31	2.08	0.22	17.47	9697	−2.08

Note: No Spring samples of $S_{1\text{-}3}$ (0 km) were collected during our sampling time due to winter ice barrier.

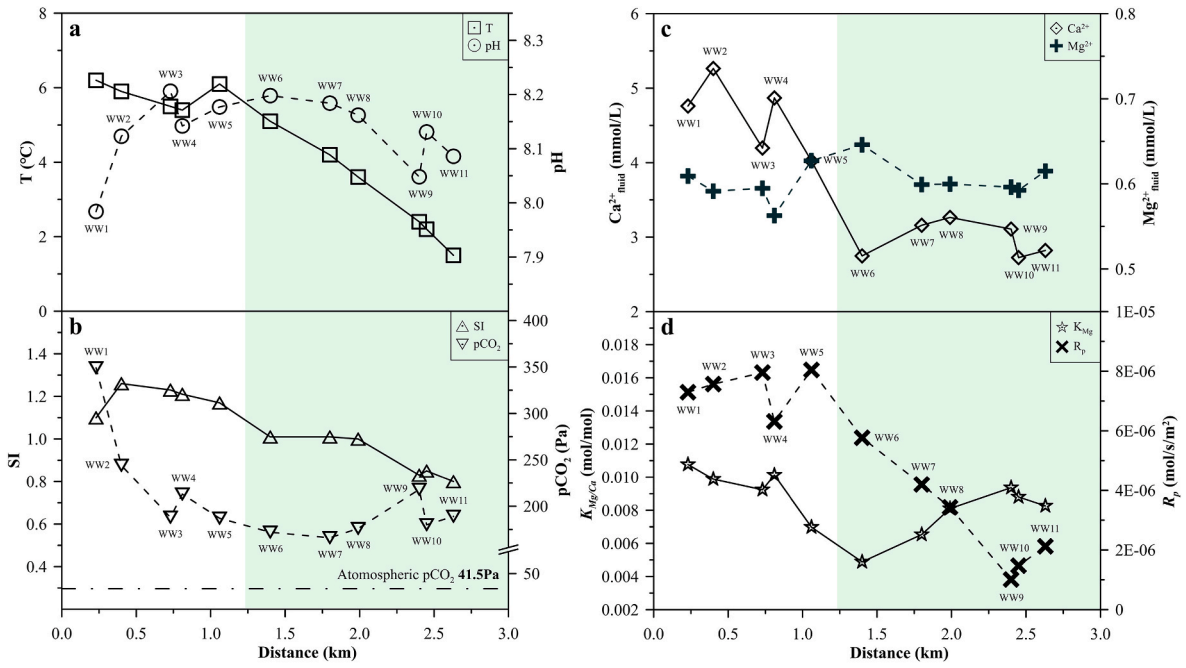

Fig. 2. Downstream evolution of a) Temperature (T) and pH value of water samples; b) saturation index (SI) and pCO_2 in water samples; c) Ca^{2+} and Mg^{2+} concentrations of water samples; and d) distribution coefficient of Mg between calcite and water ($K_{Mg/Ca}$) and deposition rate (R_p) along the canal. The light green shadowed area indicates the downstream sampling zone.

Table 2
The Mg isotope compositions of spring/stream water and travertine samples and corresponding Mg isotope fractionation factors.

Sample name	Spring/stream water				Travertine				$\Delta^{26}Mg_{calcite-water}$	2SD[a]
	$\delta^{25}Mg$ (‰)	2 SD	$\delta^{26}Mg$ (‰)	2 SD	$\delta^{25}Mg$ (‰)	2 SD	$\delta^{26}Mg$ (‰)	2 SD		
WW_1	−0.72	0.03	−1.37	0.06	−2.08	0.03	−4.02	0.01	−2.65	0.06
WW_2	−0.70	0.03	−1.35	0.01	−2.09	0.02	−4.02	0.04	−2.67	0.04
WW_3	−0.70	0.01	−1.36	0.02	−2.05	0.06	−3.95	0.08	−2.59	0.09
WW_4	−0.71	0.02	−1.35	0.03	−2.12	0.02	−4.12	0.01	−2.76	0.03
WW_5	−0.70	0.01	−1.35	0.02	−2.07	0.02	−3.97	0.03	−2.63	0.04
WW_6	−0.69	0.03	−1.32	0.03	−2.07	0.02	−4.01	0.07	−2.69	0.08
WW_7	−0.71	0.03	−1.36	0.01	−2.09	0.05	−4.02	0.08	−2.66	0.08
WW_8	−0.68	0.02	−1.33	0.01	−2.08	0.05	−4.01	0.07	−2.68	0.07
WW_9	−0.67	0.03	−1.30	0.03	−2.07	0.03	−4.02	0.06	−2.72	0.07
WW_{10}	−0.65	0.02	−1.27	0.07	−2.07	0.03	−4.02	0.07	−2.74	0.10
WW_{11}	−0.65	0.04	−1.26	0.06	−2.07	0.07	−4.02	0.09	−2.75	0.11
Standards										
Stalagmite (SS)					−2.12	0.01	−4.14	0.04		
repeat (SS)					−2.09	0.03	−4.04	0.07		
NASS-6	−0.43	0.02	−0.84	0.03						

[a] $Err\Delta^{26}Mg = [(Err\delta^{26}Mg_{calcite})^2 + (Err\delta^{26}Mg_{water})^2]^{1/2}$ (Liu and Li, 2022).

observed along the canal.

Purgstaller et al. (2016) reported that the Mg/Ca ratio of solution may affect the pathway for calcite precipitation. They discovered that when the Mg/Ca molar ratio less than 0.17 mol/mol, Mg-calcite formation occurs by direct precipitation from solution, while Mg-calcite forms *via* an intermediate Mg-rich amorphous calcium carbonate (ACC) when Mg/Ca molar ratio greater than 0.17 mol/mol (Fig. 4b). In this study, Mg/Ca ratios are less than 0.17 mol/mol for water samples WW_1 through WW_5, while are higher than 0.17 mol/mol for those from WW_6 through WW_{11}. Thus, our results appear to be consistent with the study by Purgstaller et al. (2016), and suggest log $K_{Mg/Ca}$ and log R_p may be negatively correlated during calcite precipitation *via* the ACC pathway.

This interpretation is also consistent with our observation on the variation of crystal size along the canal. As the spring/stream water flows from upstream to downstream, the crystal size of calcite precipitates become gradually smaller (Figure SI 3), with the increasing Mg molar fraction in calcite (Fig. 4b), which may be explained by the fact that calcite formation *via* an intermediate ACC pathway may result in much smaller calcite crystal size and much higher calcite Mg molar fraction (due to the substitution of ACC structure Ca^{2+} with aqueous Mg^{2+} before ACC transformed into calcite crystal entirely) (Mavromatis et al., 2017; Zou et al., 2015). Under SEM, some fine-grained calcite samples collected at WW_9 show no obvious crystal edge and grinding fracture compared with coarsely-grained calcite precipitated at WW_9 or WW_1 (Fig. 5A–C). They are morphologically similar to calcites precipitated via-ACC in the lab (Fig. 5D, from Mavromatis et al., 2017), but different in size which may be controlled by the difference of the saturation state in our study relative to previous work. Moreover, the energy dispersive spectrometer (X-MaxN80) on SEM shows that Ca and Mg are the main cations in those materials, and there is no essential difference in the spectrograms between them (Figure SI 4B1–3) and calcite

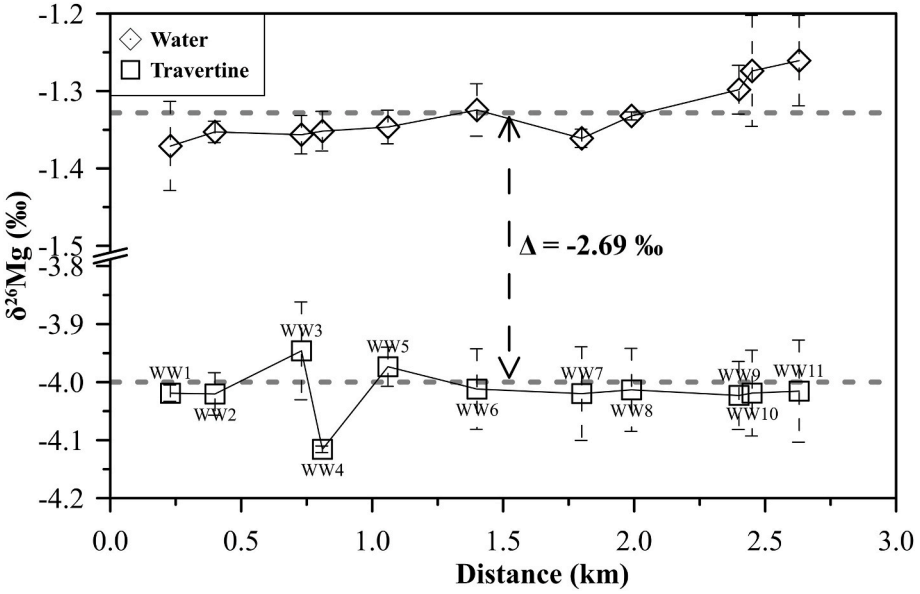

Fig. 3. Variation of Mg isotope composition ($\delta^{26}Mg$) in water and corresponding travertine samples collected along the canal at Baishuitai.

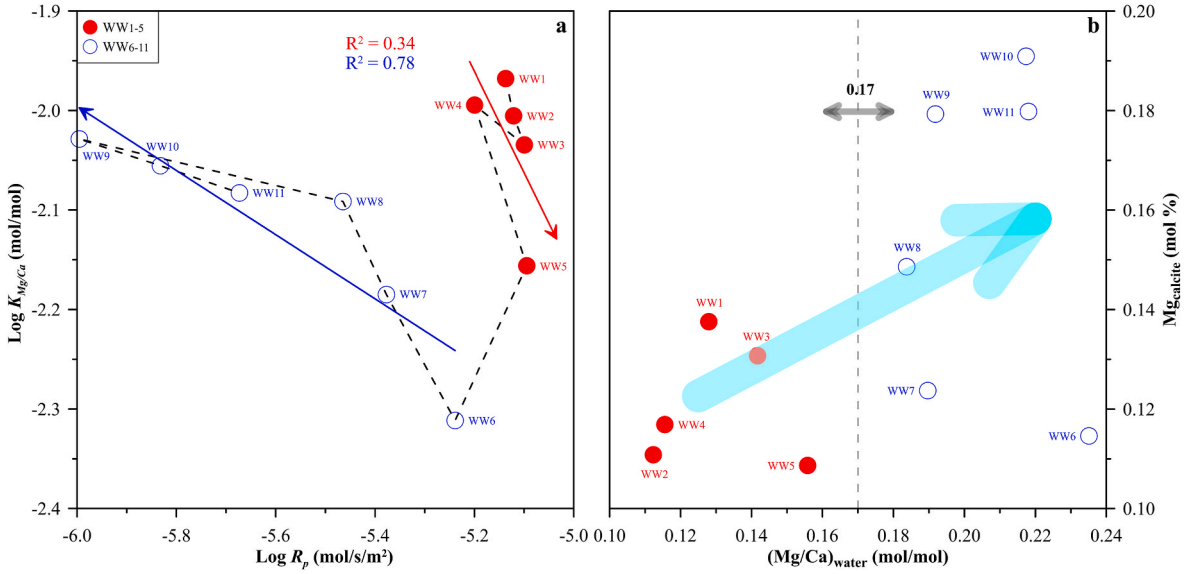

Fig. 4. a) Mg distribution coefficient plotted as a function of calcite deposition rate, the solid red and blue lines represent the fitting lines; b) Mg content of precipitates as a function of the molar Mg/Ca ratio of the spring/stream waters, the grey vertical dashed line denotes the boundary of $(Mg/Ca)_{water} = 0.17$ between the Mg-ACC and Mg-calcite for the previous experiments (Purgstaller et al., 2016), and the cyan solid line represent the tendency of the data along the canal.

(Figure SI 4B4). It is worth noting that calcite samples have no drastic change in crystal size (Figure SI 3) and the mole fraction of Mg in calcite gradually increases from WW_5 to WW_6 (Fig. 4b), which indicates likely that the change of calcite precipitation pathway may be achieved gradually, instead of instantaneous conversions. Though some coarse calcites transported upstream site such as WW_5 to WW_6 (Fig. 5, coarse-grained calcite) would contribute, this contribution must be weak as the Mg content in calcite and pCO_2 (from in-situ calcite precipitation) in water after sampling site WW_6 continuously increase (Fig. 2).

In summary, the two pathways of calcite precipitation in the canal system can be depicted in Fig. 6. At Stage I (WW_1–WW_5) where aqueous Mg/Ca molar ratio less than 0.17 in spring/stream water, the Mg/Ca ratio is too low to enable the formation and/or stabilization of ACC, and the difference between chemical potential of calcite and solution exceeds that the surface energy required for the nucleation of calcite, according to the classical nucleation theory (CNT) (e.g., Kashchiev, 2003; Yoreo and Vekilov, 2003), thus calcite minerals may precipitate directly from the spring/stream water.

At Stage II (WW_6–WW_{11}) where aqueous Mg/Ca molar ratio greater than 0.17, metastable ACC is formed first by the aggregation of ion pairs that lowers the free energy of the solid and eliminate the need to overcome the large free-energy barrier associated with the nucleation (e.g., Fernandez-Martinez et al., 2017; Gebauer et al., 2008), which consists of a nanoporous charge-separated framework formed by Ca-rich and poorly-hydrated regions that supports interconnected channels containing water and carbonate molecules but also Mg (bi)carbonate complexes (e.g., Goodwin et al., 2010; Mavromatis et al., 2017). Afterwards, the transformation of ACC to a crystalline polymorph can occur at variable reaction coordinates depending on the environmental conditions.

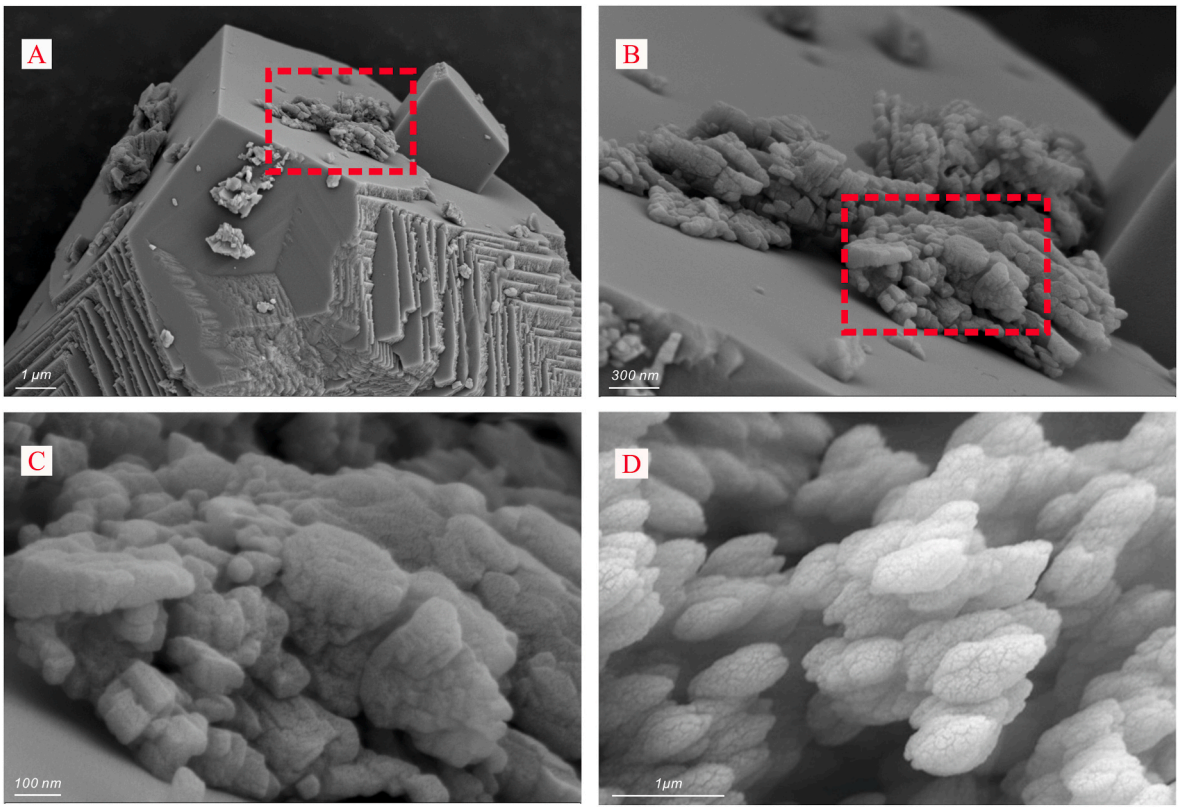

Fig. 5. (A, B, C) SEM images of sample WW_9 with different scale (red dotted boxes represent the enlarged part) and (D) calcite image precipitated via ACC reported by previous report (Mavromatis et al., 2017).

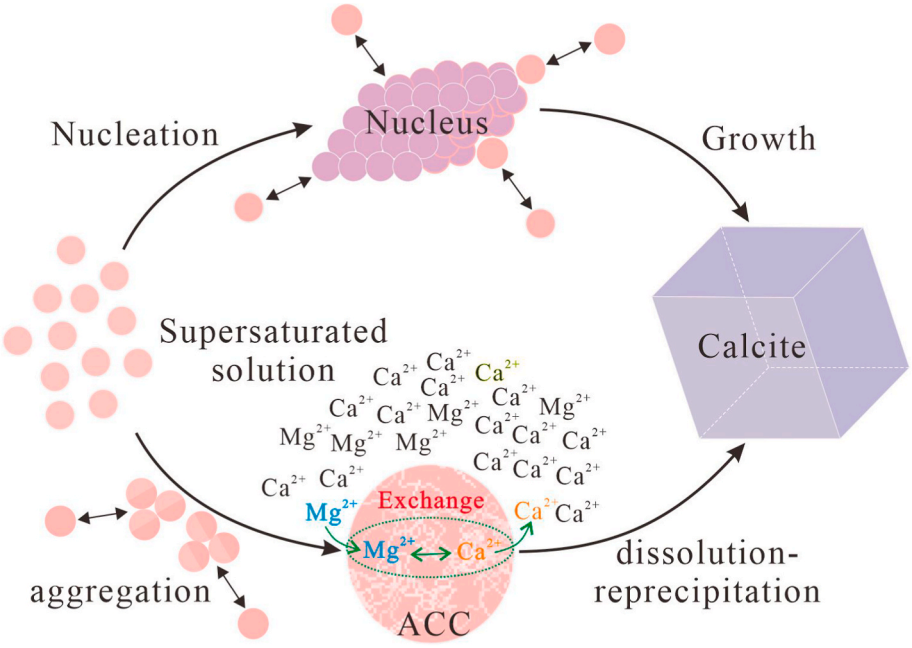

Fig. 6. Schematic representation of classical pathway of nucleation and crystallization by particle attachment (top) at Stage I, the multistage ACC calcite crystallization pathway with the underlying combined reaction progress (bottom) at Stage II.

5.2. The kinetic or equilibrium Mg isotope fractionation affected by different calcite deposition pathways

Different calcite precipitation pathways/mechanisms have significant effects on $K_{Mg/Ca}$ from upstream to downstream (Figs. 2 and 4a), which may also affect the Mg isotope fractionation between the deposited calcite and spring/stream water. Previous studies have suggested two different models to explain trace metal partition and their isotopic fractionations: surface entrapment (SE) model (Füger et al., 2019; Mavromatis et al., 2013; Watson, 2004; Watson and Liang, 1995) and

surface kinetic (SK) model (DePaolo, 2011). In the SE model, a trace element incorporated into a growing crystal can be either enriched or depleted by increasing the diffusion distance. For $K_{Mg/Ca}$ <1, the SE model predicts it should be enriched in the near surface region and thus leading to higher $K_{Mg/Ca}$ due to fast growth rate, which is consistent with previous research (e.g., Mavromatis et al., 2013; Tang et al., 2008b; Tang et al., 2012; Wang et al., 2020). However, our results show a general negative correlation between R_p and $K_{Mg/Ca}$ (Fig. 4a) at both Stage I and Stage II.

We suggest that the relationship between $K_{Mg/Ca}$ and growth rate can be likely explained by the SK model (DePaolo, 2011) as follows, which assumed that the limiting steps of ion transport and surface reaction during crystal growth can control the isotopic fractionation and the incorporation of major elements by both attachment/detachment kinetics and mass transport in the boundary diffusion layer (BDL) of calcite. At Stage I, the $\Delta^{26}Mg_{calcite\text{-}water}$ value positively correlates with R_p (Fig. 7a) and negatively correlates with $K_{Mg/Ca}$ (Fig. 7b), which is characterized by the dynamic fractionation of Mg isotopes observed in previous studies (Immenhauser et al., 2010; Mavromatis et al., 2013). Based on the SK model, the relative faster calcite precipitation rate (promoted by faster CO_2 degassing) compared with slower aqueous Mg^{2+} transmission rate in the BDL may result in the gradual decrease of Mg^{2+} concentration and increase of $\delta^{26}Mg_{BLD}$ value as ^{24}Mg (transported faster than ^{26}Mg) preferentially incorporated into calcite. This process may lead to the gradual increase of $\Delta^{26}Mg_{calcite\text{-}water}$ and decrease of $K_{Mg/Ca}$ from upstream to downstream. The kinetic Mg isotope fractionation during calcite precipitation at Stage I without prominent temperature dependency of $\Delta^{26}Mg_{calcite\text{-}water}$, as shown in our study (Fig. 8), is also consistent with results observed in previous researches (e.g., Immenhauser et al., 2010; Mavromatis et al., 2013; Mavromatis et al., 2017; Pogge von Strandmann et al., 2019; Saulnier et al., 2012).

At Stage II, the $\Delta^{26}Mg_{calcite\text{-}water}$ value has positive and negative relationships with R_p (Fig. 7a) and $K_{Mg/Ca}$ (Fig. 7b), respectively. This can be probably explained by the SK model and the calcite precipitation mechanism via ACC. When ACC nucleates through small scale dissolution-precipitation and/or diffusion processes in the network of interconnected/percolating channels (Fig. 6), the gross exchange rate of aqueous Mg^{2+} ion is much faster than the dissolution-reprecipitation rate for ACC. Thus, it is likely that the transport of Mg^{2+} to the BDL of growing calcite may not be limited, and larger $K_{Mg/Ca}$ and more ^{24}Mg entering the calcite lattice than ^{26}Mg are expected as aqueous Mg^{2+} replaces structure Ca^{2+} in the nanochannel of ACC during its stabilization time (e.g., Mavromatis et al., 2017; Schott et al., 2016). The observed $\Delta^{26}Mg_{travertine\text{-}water}$ at this stage is consistent, within error, with those of Li et al. (2012), Chen et al. (2020) and Liu and Li (2022), who have reported attainment of equilibrium Mg isotope fractionation for calcite in lab experiments (Chen et al., 2020; Li et al., 2012; Liu and Li, 2022). This may imply that the Mg isotope fractionation at this stage during precipitation of calcite *via* ACC is close to equilibrium.

5.3. Comparison with previous studies and potential applications

A statistically-significant negative correlation ($R^2 = 0.76$) between $\Delta^{26}Mg_{calcite\text{-}water}$ and $10^6/T^2$ at Stage II can be observed in Fig. 8, and described in Eq. (3)) as follows.

$$\Delta^{26}Mg_{calcite-water} = -0.26 \times 10^6/T^2 + 0.70 \quad (3)$$

where T is temperature in Kelvin.

Previous studies reported the equilibrium Mg isotope fractionation between calcite and aqueous solution in lab experiment at low (4–45 °C) and high (98–170 °C) temperature ranges (Fig. 8b, Li et al., 2012; Liu and Li, 2022). When comparing the two results obtained at temperatures ranging from 0 to 170 °C, there is a difference of −0.20 to 0.22‰, indicating one or none of these two studies actually reach Mg isotope exchange equilibrium although they may be close to Mg isotope exchange equilibrium. In comparison to the two results obtained between 2 and 5 °C, the $\Delta^{26}Mg_{calcite\text{-}water}$ values observed in this study during Stage II is 0.10–0.13‰ higher than those in Li et al. (2012), but 0.29–0.30‰ higher than those in Liu and Li (2022), suggesting it is closer to Mg isotope equilibrium than that observed in Stage I, probably due to a slower precipitation rate.

Note that all $\Delta^{26}Mg_{calcite\text{-}water}$ values determined in lab experiments (Chen et al., 2020; Li et al., 2012; Liu and Li, 2022) or observed in the field including this study are all higher than the Mg isotope fractionation factors calculated by *ab initio* methods (Fig. 8a). For instance, the equilibrium $\Delta^{26}Mg_{calcite\text{-}water}$ values from first-principles calculations range from −3.60‰ to −6.80‰ at 25 °C. These values are approximately 2–3‰ lower than the laboratory or field observations shown in Fig. 8a, which scattered between −1.70‰ and −3.50‰ (Immenhauser et al., 2010; Li et al., 2012; Mavromatis et al., 2013; Saulnier et al., 2012). The reasons for the significant discrepancies are still under debate. But it is likely to be caused by the strong hydration free energy of aqueous Mg^{2+} (Di Tommaso and de Leeuw, 2010a; Di Tommaso and de Leeuw, 2010b), the presence of intermediate phases (ACCs) (John R. Clarkson et al., 1992; Wang et al., 2012) both in lab and field, and the concentration effect during theoretical calculation (Pinilla et al., 2015;

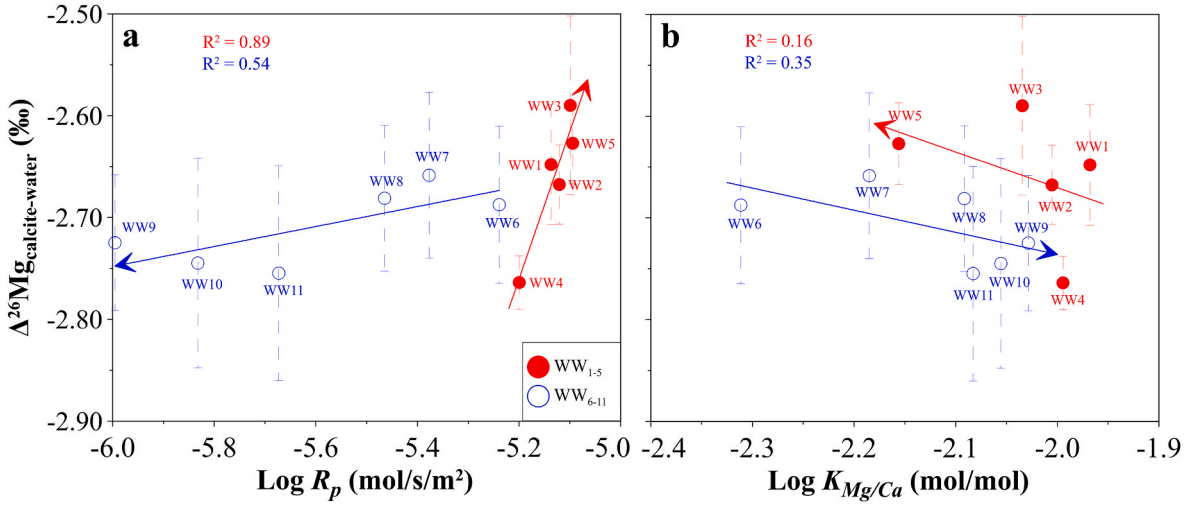

Fig. 7. The relationships of Mg isotope fractionation factors ($\Delta^{26}Mg_{calcite\text{-}water}$) *vs.* Log R_p (a) and Log $K_{Mg/Ca}$ (b) at Stage I and Stage II. The error in Mg isotope fractionation factors was calculated following the error propagation function: $Err\Delta^{26}Mg_{A\text{-}B} = [(Err\delta^{26}Mg_A)^2 + (Err\delta^{26}Mg_B)^2]^{1/2}$ (Liu and Li, 2022).

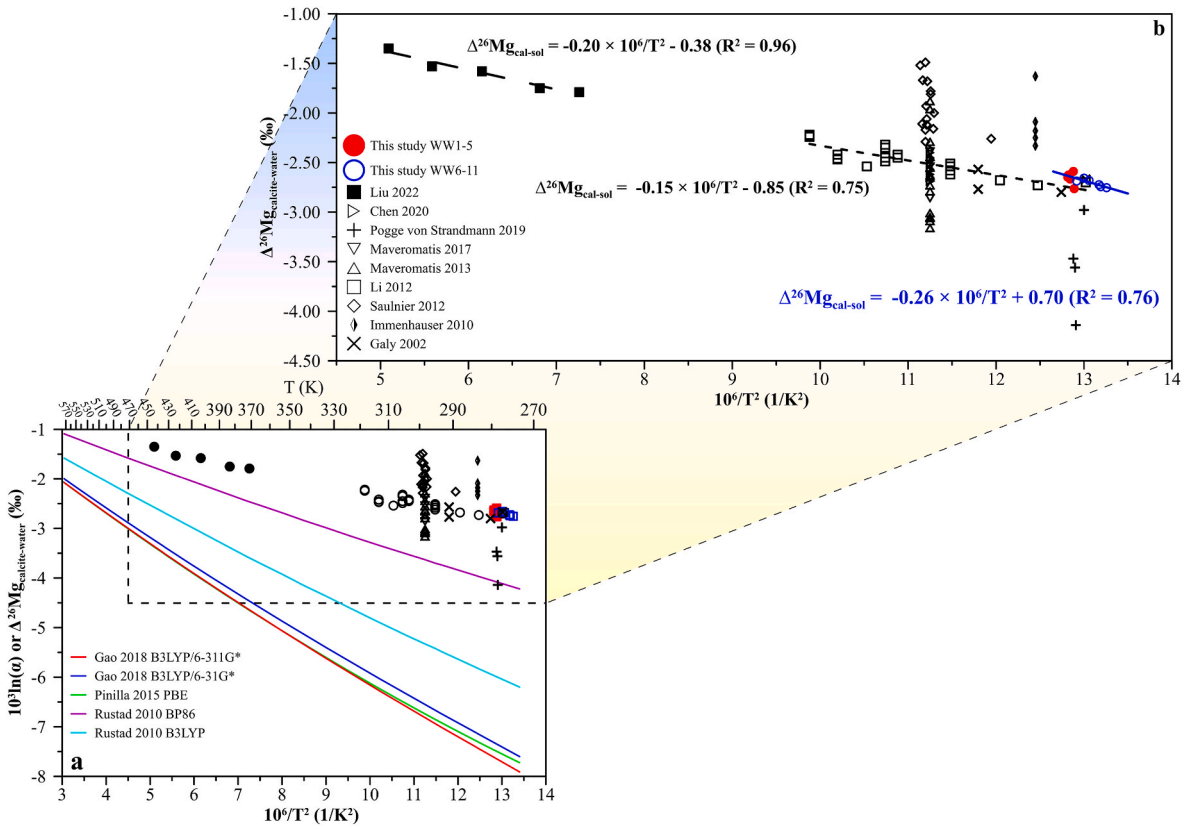

Fig. 8. Plot of Mg isotope fractionation factors between Mg-bearing calcite and solution ($\Delta^{26}Mg_{calcite-water}$) at Baishuitai as a function of $10^6/T^2$, with regression of data was performed using Grapher software. The theoretical data (Gao et al., 2018; Pinilla et al., 2015; Rustad et al., 2010) and previous experimental (Chen et al., 2020; Galy et al., 2002; Immenhauser et al., 2010; Li et al., 2012; Liu and Li, 2022; Mavromatis et al., 2013; Mavromatis et al., 2017; Pogge von Strandmann et al., 2019; Saulnier et al., 2012) are shown for comparison.

Wang et al., 2017). Further work is clearly needed to reconcile experimentally determined and calculated Mg isotope fractionation factors.

The results of this study show the strong impact of precipitation kinetics on the Mg isotope composition of calcite formed over a larger range of saturation state and Mg/Ca ratios of aqueous solution in a natural deposition environment. It implies the possibility of using Mg isotope composition of travertine deposits to reconstruct paleo-environment if $\delta^{26}Mg$ values of solution and the precipitation kinetics (e.g., Mg/Ca ratios) can be determined.

6. Conclusion

The Mg isotope compositions of the spring/stream water and deposited travertine samples in the canal system at Baishuitai (Yunnan, SW China) are investigated to understand the mechanisms controlling Mg isotope fractionation during calcite precipitation from spring/stream waters. The $\delta^{26}Mg$ value of stream water exhibits a slight increase downstream and that of the precipitated calcite varies slightly from upstream to downstream. The distinct relationship between the distribution coefficient $K_{Mg/Ca}$ and travertine deposition rate R_p in the upper-stream and down-stream can be explained by the difference in precipitation mechanism and surface reaction model. In the upper-stream when the Mg/Ca ratio of spring/stream water is low (Stage I), the Mg^{2+} transmission is limited in the boundary diffusion layer BDL, which results in the decrease of Mg^{2+} concentration, increase of $\delta^{26}Mg$ value in the BDL downstream, and the increase of $\Delta^{26}Mg_{calcite-water}$. In the down-stream when the Mg/Ca ratios of spring/stream waters are high (Stage II), the $K_{Mg/Ca}$ increases significantly due to the exchange between aqueous Mg^{2+} and structure Ca^{2+} in the nanochannel of ACC during its stabilization time. At this stage, the observed $\Delta^{26}Mg_{travertine-water}$ is the close to the equilibrium $\Delta^{26}Mg_{calcite-water}$ previously determined in the lab. The change of precipitation mechanism is also consistent with the crystal-morphology and size-distribution observed under SEM. Our results show the importance of Mg/Ca ratios of spring/stream waters on calcite precipitation mechanisms during travertine formation. It implies the possibility of using Mg isotope composition of travertine deposits to reconstruct paleo-environment if $\delta^{26}Mg$ values of solution and the precipitation kinetics (e.g., Mg/Ca ratios) can be well determined.

Declaration of competing interest

The authors declare the following financial interests/personal relationships which may be considered as potential competing interests: Chen Jiubin reports financial support was provided by the National Key Research and Development Program of China (2019YFC1804401) and the National Natural Science Foundation of China (42103008, 41973007, 41961144028, 41625012).

Data availability

Data will be made available on request.

Acknowledgments

This work was financially supported by the National Key Research and Development Program of China (2019YFC1804401), the National Natural Science Foundation of China (42103008, 41973007, 41961144028, 41625012). We thank anonymous reviewers for their constructive comments. We also thank Ying-Zeng Gong, Qi-Zhen Jin at USTC and Peng-Fei Li, Li-Xin Zhang, Xu-Nan Meng, Lin Shi at TJU for

their kind help for laboratory works.

Appendix A. Supplementary data

Supplementary data to this article can be found online at https://doi.org/10.1016/j.apgeochem.2023.105777.

References

An, Y., Wu, F., Xiang, Y., Nan, X., Yu, X., Yang, J., Yu, H., Xie, L., Huang, F., 2014. High-precision Mg isotope analyses of low-Mg rocks by MC-ICP-MS. Chem. Geol. 390, 9–21.

Andrews, J.E., 2006. Palaeoclimatic records from stable isotopes in riverine tufas: synthesis and review. Earth Sci. Rev. 75, 85–104.

Balland-Bolou-Bi, C., Bolou-Bi, E.B., Vigier, N., Mustin, C., Poszwa, A., 2019. Increased Mg release rates and related Mg isotopic signatures during bacteria-phlogopite interactions. Chem. Geol. 506, 17–28.

Berner, R.A., 1975. The role of magnesium in the crystal growth of calcite and aragonite from sea water. Geochem. Cosmochim. Acta 39, 489–504.

Black, J.R., Yin, Q.Z., Casey, W.H., 2006. An experimental study of magnesium-isotope fractionation in chlorophyll-a photosynthesis. Geochem. Cosmochim. Acta 70, 4072–4079.

Black, J.R., Yin, Q.Z., Rustad, J.R., Casey, W.H., 2007. Magnesium isotopic equilibrium in chlorophylls. J. Am. Chem. Soc. 129, 8690–8691.

Black, J.R., Epstein, E., Rains, W.D., Yin, Q.Z., Casey, W.H., 2008. Magnesium-isotope fractionation during plant growth. Environ. Sci. Technol. 42, 7831–7836.

Bolou-Bi, E.B., Poszwa, A., Leyval, C., Vigier, N., 2010. Experimental determination of magnesium isotope fractionation during higher plant growth. Geochem. Cosmochim. Acta 74, 2523–2537.

Bolou-Bi, E.B., Vigier, N., Poszwa, A., Boudot, J.-P., Dambrine, E., 2012. Effects of biogeochemical processes on magnesium isotope variations in a forested catchment in the Vosges Mountains (France). Geochem. Cosmochim. Acta 87, 341–355.

Buhl, D., Immenhauser, A., Smeulders, G., Kabiri, L., Richter, D.K., 2007. Time series δ^{26}Mg analysis in speleothem calcite: kinetic versus equilibrium fractionation, comparison with other proxies and implications for palaeoclimate research. Chem. Geol. 244, 715–729.

Chang, V.T., Williams, R.J., Makishima, A., Belshawl, N.S., O'Nions, R.K., 2004. Mg and Ca isotope fractionation during $CaCO_3$ biomineralisation. Biochem. Biophys. Res. Commun. 323, 79–85.

Chen, X.Y., Teng, F.Z., Sanchez, W.R., Romanek, C.S., Sanchez-Navas, A., Sánchez-Román, M., 2020. Experimental constraints on magnesium isotope fractionation during abiogenic calcite precipitation at room temperature. Geochem. Cosmochim. Acta 281, 102–117.

Clarkson, John R., Price, Timothy J., Adams, C.J., 1992. Role of metastable phases in the spontaneous precipitation of calcium carbonate. J. Chem. Soc., Faraday Trans. 88, 243–249.

De Boever, E., Brasier, A.T., Foubert, A., Kele, S., 2017. What do we really know about early diagenesis of non-marine carbonates? Sediment. Geol. 361, 25–51.

DePaolo, D.J., 2011. Surface kinetic model for isotopic and trace element fractionation during precipitation of calcite from aqueous solutions. Geochem. Cosmochim. Acta 75, 1039–1056.

Di Tommaso, D., de Leeuw, N.H., 2010a. First principles simulations of the structural and dynamical properties of hydrated metal ions Me^{2+} and solvated metal carbonates (me = Ca, Mg, and Sr). Cryst. Growth Des. 10, 4292–4302.

Di Tommaso, D., de Leeuw, N.H., 2010b. Structure and dynamics of the hydrated magnesium ion and of the solvated magnesium carbonates: insights from first principles simulations. Phys. Chem. Chem. Phys.: Phys. Chem. Chem. Phys. 12, 894–901.

Dong, F., Dai, Q., Jiang, Z., Chen, X., Xu, R., Zhang, Q., An, D., Li, Q., Zhang, T., Andelka, P.-M., Capezzuoli, E., Li, B., Mors, R.A., 2023. Travertine/tufa resource conservation and sustainable development call for a world-wide initiative. Appl. Geochem. 148.

Fernandez-Martinez, A., Lopez-Martinez, H., Wang, D., 2017. New Perspectives on Mineral Nucleation and Growth: from Solution Precursors to Solid Materials, vol. 11. Springer Nature, Gewerbestrasse, p. 6330 (Cham, Switzerland).

Füger, A., Konrad, F., Leis, A., Dietzel, M., Mavromatis, V., 2019. Effect of growth rate and pH on lithium incorporation in calcite. Geochem. Cosmochim. Acta 248, 14–24.

Galy, A., Bar-Matthews, M., Halicz, L., O'Nions, R.K., 2002. Mg isotopic composition of carbonate: insight from speleothem formation. Earth Planet Sci. Lett. 201, 105–115.

Galy, A., Yoffe, O., Janney, P.E., Williams, R.W., Cloquet, C., Alard, O., Halicz, L., Wadhwa, M., Hutcheon, I.D., Ramon, E., Carignan, J., 2003. Magnesium isotope heterogeneity of the isotopic standard SRM980 and new reference materials for magnesium-isotope-ratio measurements. J. Anal. Atomic Spectrom. 18, 1352–1356.

Gao, C., Cao, X., Liu, Q., Yang, Y., Zhang, S., He, Y., Tang, M., Liu, Y., 2018. Theoretical calculation of equilibrium Mg isotope fractionations between minerals and aqueous solutions. Chem. Geol. 488, 62–75.

Gebauer, D., Völkel, A., Cölfen, H., 2008. Stable prenucleation calcium carbonate clusters. Science 322, 1819–1822.

Geske, A., Zorlu, J., Richter, D.K., Buhl, D., Niedermayr, A., Immenhauser, A., 2012. Impact of diagenesis and low grade metamorphosis on isotope (δ^{26}Mg, δ^{13}C, δ^{18}O and ^{87}Sr/^{86}Sr) and elemental (Ca, Mg, Mn, Fe and Sr) signatures of Triassic sabkha dolomites. Chem. Geol. 332–333, 45–64.

Geske, A., Goldstein, R.H., Mavromatis, V., Richter, D.K., Buhl, D., Kluge, T., John, C.M., Immenhauser, A., 2015. The magnesium isotope (δ^{26}Mg) signature of dolomites. Geochem. Cosmochim. Acta 149, 131–151.

Goodwin, A.L., Michel, F.M., Phillips, B.L., Keen, D.A., Dove, M.T., Reeder, R.J., 2010. Nanoporous structure and medium-range order in synthetic amorphous calcium carbonate. Chem. Mater. 22, 3197–3205.

Gradziński, M., 2010. Factors controlling growth of modern tufa: results of a field experiment. Geological Society, London, Special Publications 336, 143–191.

Immenhauser, A., Buhl, D., Richter, D., Niedermayr, A., Riechelmann, D., Dietzel, M., Schulte, U., 2010. Magnesium-isotope fractionation during low-Mg calcite precipitation in a limestone cave–Field study and experiments. Geochem. Cosmochim. Acta 74, 4346–4364.

Kano, A., Okumura, T., Takashima, C., Shiraishi, F., 2019. Geomicrobiological Properties and Processes of Travertine (With a Focus on Japanese Sites). Springer, Singapore.

Kashchiev, D., 2003. Thermodynamically consistent description of the work to form a nucleus of any size. J. Chem. Phys. 118, 1837–1851.

Kele, S., Breitenbach, S.F.M., Capezzuoli, E., Meckler, A.N., Ziegler, M., Millan, I.M., Kluge, T., Deák, J., Hanselmann, K., John, C.M., Yan, H., Liu, Z., Bernasconi, S.M., 2015. Temperature dependence of oxygen- and clumped isotope fractionation in carbonates: a study of travertines and tufas in the 6–95°C temperature range. Geochem. Cosmochim. Acta 168, 172–192.

Kimmig, S.R., Holmden, C., Bélanger, N., 2018. Biogeochemical cycling of Mg and its isotopes in a sugar maple forest in Québec. Geochem. Cosmochim. Acta 230, 60–82.

Li, W., Chakraborty, S., Beard, B.L., Romanek, C.S., Johnson, C.M., 2012. Magnesium isotope fractionation during precipitation of inorganic calcite under laboratory conditions. Earth Planet Sci. Lett. 333–334, 304–316.

Liu, C., Li, W., 2022. Magnesium isotope fractionation between calcite and aqueous solutions under elevated temperatures of 98–170°C. Geochem. Cosmochim. Acta 344, 160–177.

Liu, Z., Zhang, M., Li, Q., You, S., 2003. Hydrochemical and isotope characteristics of spring water and travertine in the Baishuitai area (SW China) and their meaning for paleoenvironmental reconstruction. Environ. Geol. 44, 698–704.

Liu, Z., Li, H., You, C., Wan, N., Sun, H., 2006a. Thickness and stable isotopic characteristics of modern seasonal climate-controlled sub-annual travertine laminas in a travertine-depositing stream at Baishuitai, SW China: implications for paleoclimate reconstruction. Environ. Geol. 51, 257–265.

Liu, Z., Li, Q., Sun, H., Liao, C., Li, H., Wang, J., Wu, K., 2006b. Diurnal variations of hydrochemistry in a travertine-depositing stream at Baishuitai, Yunnan, SW China. Aquat. Geochem. 12, 103–121.

Liu, Z., Sun, H., Lu, B., Liu, X., Ye, W., Cheng, Z., 2010. Wet-dry seasonal variations of hydrochemistry and carbonate precipitation rates in a travertine-depositing canal at Baishuitai, Yunnan, SW China: implications for the formation of biannual laminae in travertine and for climatic reconstruction. Chem. Geol. 273, 258–266.

Liu, C., Wang, Z., Raub, T.D., 2013. Geochemical constraints on the origin of marinoan cap dolostones from nuccaleena formation, south Australia. Chem. Geol. 351, 95–104.

Liu, C., Wang, Z., Macdonald, F.A., 2018. Sr and Mg isotope geochemistry of the basal Ediacaran cap limestone sequence of Mongolia: implications for carbonate diagenesis, mixing of glacial meltwaters, and seawater chemistry in the aftermath of Snowball Earth. Chem. Geol. 491, 1–13.

Mavromatis, V., Gautier, Q., Bosc, O., Schott, J., 2013. Kinetics of Mg partition and Mg stable isotope fractionation during its incorporation in calcite. Geochem. Cosmochim. Acta 114, 188–203.

Mavromatis, V., Purgstaller, B., Dietzel, M., Buhl, D., Immenhauser, A., Schott, J., 2017. Impact of amorphous precursor phases on magnesium isotope signatures of Mg-calcite. Earth Planet Sci. Lett. 464, 227–236.

Mavromatis, V., Power, I.M., Harrison, A.L., Beinlich, A., Dipple, G.M., Bénézeth, P., 2021. Mechanisms controlling the Mg isotope composition of hydromagnesite-magnesite playas near Atlin, British Columbia, Canada. Chem. Geol. 579, 120325.

Minissale, A., Kerrick, D.M., Magro, G., Murrell, M.T., Paladini, M., Rihs, S., Sturchio, N. C., Tassi, F., Vaselli, O., 2002. Geochemistry of Quaternary travertines in the region north of Rome (Italy): structural, hydrologic and paleoclimatic implications. Earth Planet Sci. Lett. 203, 709–728.

Mutlu, H., Karabacak, V., Deniz, K., Erkkila, B.R., 2022. Multiple geochemical, mineralogical and isotopic approaches to constrain the deposition conditions of Gazlıgöl travertines, western Turkey. Appl. Geochem. 139.

Opfergelt, S., Burton, K.W., Georg, R.B., West, A.J., Guicharnaud, R.A., Sigfusson, B., Siebert, C., Gislason, S.R., Halliday, A.N., 2014. Magnesium retention on the soil exchange complex controlling Mg isotope variations in soils, soil solutions and vegetation in volcanic soils, Iceland. Geochem. Cosmochim. Acta 125, 110–130.

Pentecost, A., 2005. Travertine. Springer-Verlag, Berlin, Heidelberg.

Pinilla, C., Blanchard, M., Balan, E., Natarajan, S.K., Vuilleumier, R., Mauri, F., 2015. Equilibrium magnesium isotope fractionation between aqueous Mg^{2+} and carbonate minerals: insights from path integral molecular dynamics. Geochem. Cosmochim. Acta 163, 126–139.

Pogge von Strandmann, P.A.E., 2008. Precise magnesium isotope measurements in core top planktic and benthic foraminifera. Geochem. Geophys. Geosyst. 9, 1–13.

Pogge von Strandmann, P.A.E., Olsson, J., Luu, T.-H., Gislason, S.R., Burton, K.W., 2019. Using Mg isotopes to estimate natural calcite compositions and precipitation rates during the 2010 Eyjafjallajökull eruption. Front. Earth Sci. 7, 1–9.

Purgstaller, B., Mavromatis, V., Immenhauser, A., Dietzel, M., 2016. Transformation of Mg-bearing amorphous calcium carbonate to Mg-calcite–In situ monitoring. Geochem. Cosmochim. Acta 174, 180–195.

Ra, K., Kitagawa, H., 2007. Magnesium isotope analysis of different chlorophyll forms in marine phytoplankton using multi-collector ICP-MS. J. Anal. Atomic Spectrom. 22, 817–821.

Ra, K., Kitagawa, H., Shiraiwa, Y., 2010a. Mg isotopes and Mg/Ca values of coccoliths from cultured specimens of the species Emiliania huxleyi and Gephyrocapsa oceanica. Mar. Micropaleontol. 77, 119–124.
Ra, K., Kitagawa, H., Shiraiwa, Y., 2010b. Mg isotopes in chlorophyll-a and coccoliths of cultured coccolithophores (Emiliania huxleyi) by MC-ICP-MS. Mar. Chem. 122, 130–137.
Riechelmann, S., Buhl, D., Schröder-Ritzrau, A., Riechelmann, D.F.C., Richter, D.K., Vonhof, H.B., Wassenburg, J.A., Geske, A., Spötl, C., Immenhauser, A., 2012. The magnesium isotope record of cave carbonate archives. Clim. Past 8, 1849–1867.
Rustad, J.R., Casey, W.H., Yin, Q.Z., Bylaska, E.J., Felmy, A.R., Bogatko, S.A., Jackson, V. E., Dixon, D.A., 2010. Isotopic fractionation of Mg^{2+}(aq), Ca^{2+}(aq), and Fe^{2+}(aq) with carbonate minerals. Geochem. Cosmochim. Acta 74, 6301–6323.
Saenger, C., Wang, Z., 2014. Magnesium isotope fractionation in biogenic and abiogenic carbonates: implications for paleoenvironmental proxies. Quat. Sci. Rev. 90, 1–21.
Saulnier, S., Rollion-Bard, C., Vigier, N., Chaussidon, M., 2012. Mg isotope fractionation during calcite precipitation: an experimental study. Geochem. Cosmochim. Acta 91, 75–91.
Schott, J., Mavromatis, V., Fujii, T., Pearce, C.R., Oelkers, E.H., 2016. The control of carbonate mineral Mg isotope composition by aqueous speciation: theoretical and experimental modeling. Chem. Geol. 445, 120–134.
Sun, H., Liu, Z., 2010. Wet–dry seasonal and spatial variations in the $\delta^{13}C$ and $\delta^{18}O$ values of the modern endogenic travertine at Baishuitai, Yunnan, SW China and their paleoclimatic and paleoenvironmental implications. Geochem. Cosmochim. Acta 74, 1016–1029.
Sun, H., Liu, Z., Yan, H., 2014. Oxygen isotope fractionation in travertine-depositing pools at Baishuitai, Yunnan, SW China: effects of deposition rates. Geochem. Cosmochim. Acta 133, 340–350.
Sun, H., Shen, C.C., Wu, C.-C., Chen, B., Yin, J., Yan, H., Dong, J., An, D., Tang, S., Zhang, Q., 2022. Subannual-to-biannual-resolved travertine record of Asian Summer Monsoon dynamics in the early Holocene at the eastern margin of Tibetan Plateau. Appl. Geochem. 141.
Tang, J., Dietzel, M., Böhm, F., Köhler, S.J., Eisenhauer, A., 2008a. Sr^{2+}/Ca^{2+} and $^{44}Ca/^{40}Ca$ fractionation during inorganic calcite formation: II. Ca isotopes. Geochem. Cosmochim. Acta 72, 3733–3745.
Tang, J., Köhler, S.J., Dietzel, M., 2008b. Sr^{2+}/Ca^{2+} and $^{44}Ca/^{40}Ca$ fractionation during inorganic calcite formation: I. Sr incorporation. Geochem. Cosmochim. Acta 72, 3718–3732.
Tang, J., Niedermayr, A., Kohler, S.J., Bohm, F., Kisakurek, B., Eisenhauer, A., Dietzel, M., 2012. Sr^{2+}/Ca^{2+} and $^{44}Ca/^{40}Ca$ fractionation during inorganic calcite formation: III. Impact of salinity/ionic strength. Geochem. Cosmochim. Acta 77, 432–443.
Teng, F.Z., 2017. Magnesium isotope geochemistry. Rev. Mineral. Geochem. 82, 219–287.
Teng, F.Z., Li, W.Y., Ke, S., Yang, W., Liu, S.A., Sedaghatpour, F., Wang, S.J., Huang, K.J., Hu, Y., Ling, M.X., Xiao, Y., Liu, X.M., Li, X.W., Gu, H.O., Sio, C.K., Wallace, D.A., Su, B.X., Zhao, L., Chamberlin, J., Harrington, M., Brewer, A., 2015. Magnesium isotopic compositions of international geological reference materials. Geostand. Geoanal. Res. 39, 329–339.
Tipper, E.T., Gaillardet, J., Louvat, P., Capmas, F., White, A.F., 2010. Mg isotope constraints on soil pore-fluid chemistry: evidence from Santa Cruz, California. Geochem. Cosmochim. Acta 74, 3883–3896.
Wang, D., Hamm, L.M., Bodnar, R.J., Dove, P.M., 2012. Raman spectroscopic characterization of the magnesium content in amorphous calcium carbonates. J. Raman Spectrosc. 43, 543–548.
Wang, H., Yan, H., Liu, Z., 2014. Contrasts in variations of the carbon and oxygen isotopic composition of travertines formed in pools and a ramp stream at Huanglong Ravine, China: implications for paleoclimatic interpretations. Geochem. Cosmochim. Acta 125, 34–48.
Wang, W., Qin, T., Zhou, C., Huang, S., Wu, Z., Huang, F., 2017. Concentration effect on equilibrium fractionation of Mg-Ca isotopes in carbonate minerals: insights from first-principles calculations. Geochem. Cosmochim. Acta 208, 185–197.
Wang, Z., Chen, J., Cai, H., Yuan, W., Yuan, S., 2020. Coprecipitation of metal ions into calcite: an estimation of partition coefficients based on field investigation. Acta Geochimica 40, 1–11.
Watkins, J.M., Hunt, J.D., Ryerson, F.J., DePaolo, D.J., 2014. The influence of temperature, pH, and growth rate on the $\delta^{18}O$ composition of inorganically precipitated calcite. Earth Planet Sci. Lett. 404, 332–343.
Watson, E.B., 2004. A conceptual model for near-surface kinetic controls on the trace-element and stable isotope composition of abiogenic calcite crystals. Geochem. Cosmochim. Acta 68, 1473–1488.
Watson, E.B., Liang, Y., 1995. A simple model for sector zoning in slowly growing crystals: implications for growth rate and lattice diffusion, with emphasis on accessory minerals in crustal rocks. Am. Mineral. 80, 1179–1187.
Wombacher, F., Eisenhauer, A., Böhm, F., Gussone, N., Regenberg, M., Dullo, W.C., Rüggeberg, A., 2011. Magnesium stable isotope fractionation in marine biogenic calcite and aragonite. Geochem. Cosmochim. Acta 75, 5797–5818.
Wrobel, K., Karasinski, J., Tupys, A., Arroyo Negrete, M.A., Halicz, L., Wrobel, K., Bulska, E., 2020. Magnesium-isotope fractionation in chlorophyll-a extracted from two plants with different pathways of carbon fixation (C3, C4). Molecules 25, 1–12.
Yan, H., Sun, H., Liu, Z., 2012. Equilibrium vs. kinetic fractionation of oxygen isotopes in two low-temperature travertine-depositing systems with differing hydrodynamic conditions at Baishuitai, Yunnan, SW China. Geochem. Cosmochim. Acta 95, 63–78.
Yan, H., Schmitt, A.D., Liu, Z., Gangloff, S., Sun, H., Chen, J., Chabaux, F., 2016. Calcium isotopic fractionation during travertine deposition under different hydrodynamic conditions: examples from Baishuitai (Yunnan, SW China). Chem. Geol. 426, 60–70.
Yan, H., Liu, Z., Sun, H., 2017. Effect of in-stream physicochemical processes on the seasonal variations in $\delta^{13}C$ and $\delta^{18}O$ values in laminated travertine deposits in a mountain stream channel. Geochem. Cosmochim. Acta 202, 179–189.
Yoreo, J.J.D., Vekilov, P.G., 2003. Principles of crystal nucleation and growth. Rev. Mineral. Geochem. 54, 57–93.
Young, E.D., Galy, A., 2004. The isotope geochemistry and cosmochemistry of magnesium. Rev. Mineral. Geochem. 55, 197–230.
Zhao, T., Liu, W., Xu, Z., Sun, H., Zhou, X., Zhou, L., Zhang, J., Zhang, X., Jiang, H., Liu, T., 2019. The influence of carbonate precipitation on riverine magnesium isotope signals: new constrains from Jinsha River Basin, Southeast Tibetan Plateau. Geochem. Cosmochim. Acta 248, 172–184.
Zou, Z., Bertinetti, L., Politi, Y., Jensen, A.C.S., Weiner, S., Addadi, L., Fratzl, P., Habraken, W.J.E.M., 2015. Opposite particle size effect on amorphous calcium carbonate crystallization in water and during heating in air. Chem. Mater. 27, 4237–4246.